Chapter 11

THEORY OF PHOTOELECTRON EMISSION FROM AN X-RAY INTERFERENCE FIELD

IVAN A. VARTANYANTS

Deutsches Electronen Synchrotron, DESY,
Notkestraße 85,
D-22607 Hamburg, Germany
National Research Nuclear University, "MEPhI",
115409, Moscow, Russia

JÖRG ZEGENHAGEN

European Synchrotron Radiation Facility,
6 rue Jules Horowitz,
F-38000 Grenoble, France

In this chapter, we will present the theory for the photoelectron emission from an X-ray interference field. The dipole approximation holds astonishingly well, even for hard X-rays, as far as the magnitude of the transition matrix element is concerned. However, the forward–backward asymmetry caused already by higher order multipole terms cannot be neglected when the photoelectron is emitted by the coherent action of two X-ray waves travelling in different directions. We will explicitly elaborate the underlying theory and how corresponding data are analyzed. Furthermore, we will briefly describe the theory behind the X-ray standing wave excited photoemission of valence band electrons.

11.1. Introduction

During the last decade it has become clear by theoretical considerations[1,2] and experimental investigations[3] that an accurate description of the angular resolved hard X-ray photoelectron spectroscopy (HAXPES)[4] has

to go beyond the traditionally used dipole approximation and higher-order multipole terms in the photoelectron emission (PE) process have to be included. However, it was not immediately realized how important these non-dipole contributions will be in the case of certain applications of the X-ray standing wave (XSW) technique.[5,6]

If the dipole approximation is valid, the intensity of the PE from an atom exposed to an X-ray interference field (XIF) will be exactly proportional to the intensity of the standing wave at the position of the atom.[6,7] By normalization, the proportionality factor cross-section cancels out. With the position of the standing wave field known, atomic positions can be deduced from the characteristic yield, e.g., employing the dynamical theory of X-ray diffraction for single crystals. However, this simple relationship fails in certain cases. First, if angular resolved PE and π-polarized radiation are considered,[8,9] two E-field vectors are not collinear and consequently the dipole emission lobes from the two X-ray waves do not point in the same direction any longer. Second, and this is the topic of this chapter, when non-dipole terms in the photoelectric process are appreciable, the emission lobes are no longer symmetric around the E-field vectors. Thus, higher-order terms have to be taken into account and the formalism for the XSW analysis has to be revised.

In the last years, several publications addressed this questions from a theoretical[9–12] and experimental[13–17] point of view. If non-dipole terms are taken into account, the expression for the photoelectron yield describing the emission from a particular atomic site has to be generalized and can no longer be described by the well-known expression of the intensity of the XSW.[18] For certain cases it became also clear that these non-dipole contributions are by no means negligible and must be taken into account if the XSW analysis is not to be flawed. However, on the other hand, if multipole contributions are significant (more than several percent) they can directly be determined by the XSW technique and unique information about the scattering process can be extracted.

The XSW method is particularly powerful for the analysis of the structure of adsorbates on crystalline substrates,[6] and photoelectron spectroscopy is here an important tool. Thus, it is important to know how non-dipole terms are to be taken into account in order to obtain the correct positions of adsorbates. These questions will be addressed in the present chapter and we will present an overview of theoretical considerations and experimental studies of non-dipole contributions in the angular resolved PE in the presence of an XSW.

11.2. Photoelectron Scattering Process by a Single Electromagnetic Wave

Within the frame of non-relativistic quantum mechanics for a one-electron, one-photon linear process in first-order perturbation theory the interaction Hamiltonian between the electron and the electromagnetic field, responsible for the photo-absorption, can be written as,

$$\hat{\mathcal{H}}_{\text{int}} = -\frac{1}{c}\int \hat{\mathbf{j}}(\mathbf{r})\hat{\mathbf{A}}(\mathbf{r})dV. \tag{11.1}$$

Here $\hat{\mathbf{A}}(\mathbf{r})$ is the vector potential of the electromagnetic field and $\hat{\mathbf{j}}(\mathbf{r})$ is the current operator

$$\hat{\mathbf{j}}(\mathbf{r}) = \frac{e_0}{2m}[\hat{\mathbf{p}}\delta(\mathbf{r}-\mathbf{r_e}) + \delta(\mathbf{r}-\mathbf{r_e})\hat{\mathbf{p}}],$$

where e_0, m and $\mathbf{r_e}$ are the charge, mass, and coordinate, respectively, of an electron and $\hat{\mathbf{p}} = -i\hbar\nabla$ is the momentum operator.[a]

In the analysis we will use a one-electron central potential model for the description of the photo-excitation process. In case of the photoionization of a many-electron atom, we have to sum the expression for the current operator $\hat{j}(\mathbf{r})$ over the coordinates of all electrons and to chose a many-electron antisymmetric wave function for an atom. Though simplified, a one-electron model gives qualitatively, and even quantitatively, a good description of the process at high energies and, even more essential for the further considerations, the general properties of the photoelectron angular distribution in the central potential model are conserved in the many-electron description.[19] However, for open-shell atoms and photoelectron energies near threshold, when the interaction between the photoelectron and the residual ion is dependent on the ionic term level as well as on the orbital and spin angular momentum coupling of the ion-electron system, more sophisticated theories have to be applied.[20]

In case of the photoelectric process, a photon of energy $E_\gamma = \hbar\omega$ is absorbed by an atom and the energy E_γ is transferred to an electron, which is excited from the ground state $|i\rangle$ to a final state $|f\rangle$. In the following, we restrict ourselves to the case that this final state is unbound. In the non-relativistic limit the differential cross-section for the absorption of a photon

[a]For our future treatment it is more convenient to use the electric field vector $\mathbf{E}$ rather then the vector potential $\mathbf{A}$. In case of the Coulomb gauge of the electromagnetic field, they are connected by the relation, $\mathbf{E} = -\frac{1}{c}\frac{\partial \mathbf{A}}{\partial t}$.

plane wave $\mathbf{E} = \mathbf{e}E_0 \exp(i\mathbf{kr} - i\omega t)$ by an atom and the concomitant ejection of a bound electron into a continuum state is determined by the matrix element M_{fi} of the process and can be written in the following form,[21]

$$\frac{d\sigma(\vartheta_p,\phi_p)}{d\Omega} \propto |M_{fi}|^2, \tag{11.2}$$

$$M_{fi} = \langle f| \exp(i\mathbf{k}\cdot\mathbf{r})(\mathbf{e}\cdot\hat{\mathbf{p}})|i\rangle. \tag{11.3}$$

Here ϑ_p and ϕ_p are the spherical angles of the direction of the escaping photoelectron $\mathbf{k}_p$ (see Fig. 11.1). The incident photon is described by the wave vector $\mathbf{k}$. We define here its magnitude different from the definition in other chapters as $|\mathbf{k}| = 2\pi/\lambda$ (it simplifies the wave equations $\exp(i\mathbf{kr})$ saving the factor 2π in the exponential). The polarization direction of the electric field vector is described by the unit vector $\mathbf{e}$. The total cross-section is obtained from (11.2) and (11.3) by integrating over the whole spatial angle Ω of the escaping photoelectron.

11.2.1. *Non-dipole contributions*

In the long wavelength limit $\lambda \gg a$ (where a is the average size of the electron-bound state orbital) it is clear that the retardation factor $\exp(i\mathbf{kr})$ of the matrix element M_{fi} (11.3) can be expanded in a Taylor series

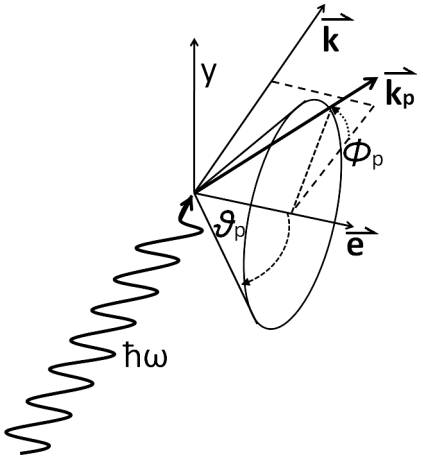

Fig. 11.1. Geometric relationships for the PE process from an atom for an electromagnetic wave with the wave vector $\mathbf{k}$ pointing in the x-direction and the polarization vector $\mathbf{e}$ pointing in the z-direction. The direction of the escaping photoelectron with the propagation vector $\mathbf{k}_p$ is characterized by the spherical angles ϑ_p and ϕ_p.

$\exp(i\mathbf{kr}) = 1 + i\mathbf{kr} - \frac{1}{2}(\mathbf{kr})^2 - \cdots$ which is equivalent to a multipole expansion. The first term gives electric dipole ($E1$) and the second term electric quadrupole ($E2$) and magnetic dipole ($M1$) transitions. We will neglect magnetic transitions for the photo-emission process in the following[b] and take into account only electric ($E1, E2, E3$, etc.) transitions. Neglecting also octupole ($E3$) and higher contributions, we get for the matrix element in (11.3)

$$M_{fi}(\mathbf{s}) = M_{fi}^{D} + M_{fi}^{Q}(\mathbf{s}), \tag{11.4}$$

where $\mathbf{s} = \mathbf{k}/|\mathbf{k}|$ is the unit vector in the direction of the photon propagation. Only the second term corresponding to quadrupole transitions depends on the propagation vector $\mathbf{s}$ but both terms are in general complex numbers and can interfere with each other. Keeping just the main terms we obtain for the photoelectron cross-section,

$$\frac{d\sigma(\vartheta_p, \phi_p)}{d\Omega} \propto \left|M_{fi}^{D}\right|^2 + 2\ \mathrm{Re}[(M_{fi}^{D})^* M_{fi}^{Q}(\mathbf{s})]. \tag{11.5}$$

It was shown in (11.2) that for linearly polarized photons, this general expression for the photoelectron angular distribution may be conveniently parametrized in the following way:

$$\frac{d\sigma(\vartheta_p, \phi_p)}{d\Omega} = (\sigma/4\pi)\{1 + \beta P_2(\mathbf{e}\cdot\mathbf{n}_p) + [\delta + \gamma(\mathbf{e}\cdot\mathbf{n}_p)^2](\mathbf{s}\cdot\mathbf{n}_p)\}, \tag{11.6}$$

where $P_2(z) = 0.5(3x^2 - 1)$ is the second-order Legendre polynomial, and $\mathbf{n}_p = \mathbf{k}_p/|\mathbf{k}_p|$ is a unit vector along the direction of the ejected electron characterized by the momentum $\mathbf{k}_p$ with the magnitude $k_p = |\mathbf{k}_p|$. In Eq. (11.6), the parameter β is the dipole asymmetry parameter, and γ and δ are two additional parameters that take into account non-dipole contributions. The values of parameters β, γ and δ depend on the type of atom, sub-shell and photoelectron energy. The term $\mathbf{s}\cdot\mathbf{n}_p$, which is caused by the quadrupole contribution, introduces a forward–backward asymmetry in the PE process with respect to the photon direction $\mathbf{s}$. Values of parameters β, γ and δ are given for the photoelectron energies E_{ph} from 100 to 5000 eV in Ref. 22.

[b]For a central-field model and a one-electron approximation, the magnetic transition probability for the photo-effect is equal to zero due to the orthogonality of the initial and final state radial wave functions. If core relaxations are taken into account, the probability for magnetic transitions does not vanish but is much smaller than for electric quadrupole contributions.[1,2]

In the non-relativistic approximation and the photo-ejection from an initial state with the orbital angular momentum l, the parameter β is given by the formula,[19,c]

$$\beta = \frac{l(l-1)(\rho^D_{l-1})^2 + (l+1)(l+2)(\rho^D_{l+1})^2 - 6l(l+1)\rho^D_{l+1}\rho^D_{l-1}\cos(\delta_{l+1} - \delta_{l-1})}{(2l+1)[l(\rho^D_{l-1})^2 + (l+1)(\rho^D_{l+1})^2]}. \tag{11.7}$$

Here, the $\rho^D_{l\pm1}$ and $\delta_{l\pm1}$ denote the radial dipole matrix elements, and phase shifts, respectively[19] (see also further below). The value of β ranges from $\beta = 2$ to $\beta = -1$.

We will first consider only dipole transitions and thus neglect γ and δ. For the limiting case $\beta = 2$, Eq. (11.7) has then a $\cos^2\vartheta_p$ (where ϑ_p is the angle between the vectors $\mathbf{e}$ and $\mathbf{n}_p$) distribution which is peaked at the polarization vector of the radiation field; for the other limiting case $\beta = -1$, the angular distribution has a $\sin^2\vartheta_p$ distribution peaked in a plane at right angles to the polarization vector of the radiation field; and for the case $\beta = 0$, the angular distribution is isotropic.

In case of multipole contributions and s-initial states, expression (11.6) for the angular distribution of the photoelectron yield is also simplified. Since in this case relativistic effects can practically be neglected, and to a very good approximation $\beta = 2$ and $\delta = 0$, which gives for the cross-section

$$\frac{d\sigma(\vartheta_p, \phi_p)}{d\Omega} = (\sigma/4\pi)(\mathbf{e}\cdot\mathbf{n}_p)^2[3 + \gamma(\mathbf{s}\cdot\mathbf{n}_p)]. \tag{11.8}$$

Consequently, for s-initial states, non-dipole effects are practically determined by one parameter γ only. For $\gamma > 0$ the photoelectron distribution is shifted forward and for $\gamma < 0$ it is shifted backward with respect to the X-ray direction.

Non-dipole contributions were experimentally tested in a number of experiments with atomic (inert) gases[3] and agreed well with theoretical calculations. It was demonstrated[3] that the ratio of the forward to backward intensities could reach 1.6. That means that non-dipole effects in high-energy angular resolved PE are important and cannot be neglected. In the simplest case, knowledge of these parameters can be used to optimize

[c]The expression for β (11.7) is obtained for a one-electron central potential model. A more general treatment[19] proves that for the photo-excitation process in an atom with many electrons described by LS coupling the angular distribution is equivalent to that of an one-electron atom.

the signal for an experiment, or to evaluate cross-sections accurately.[23] However, as we will show in the following, not taking these parameters properly into account can lead to a seriously erroneous analysis of XSW data. In principle, terms higher than quadrupole can also be taken into account.[24] However, their contribution to the photoelectron yield is expected to be small, usually less then one percent.[25]

11.3. Generalized Expression for the Photoelectron Yield from Atoms within the XSW

The total electric field in the region of two coherently related electromagnetic plane waves can be expressed (for each polarization state) as

$$\mathbf{E}(\mathbf{r}) = (\mathbf{e_0} E_0 e^{i\mathbf{k_0}\cdot\mathbf{r}} + \mathbf{e_h} E_h e^{i\mathbf{k_h}\cdot\mathbf{r}}) e^{-i\omega t}, \tag{11.9}$$

where E_0 and E_h are the complex amplitudes of the electric field, with the polarization unit-vectors $\mathbf{e_0}$ and $\mathbf{e_h}$.The two propagation vectors $\mathbf{k_0}$ and $\mathbf{k_h}$ are satisfying the condition $|\mathbf{k_h}| = |\mathbf{k_0}|$ and are connected by the vector $\mathbf{h}$ via $\mathbf{k_h} = \mathbf{k_0} + \mathbf{h}$ ($\mathbf{h} = 2\pi\mathbf{H}$ with $\mathbf{H}$ used in other chapters).

The wave field intensity at any point $\mathbf{r}$ for the different polarization states is determined by,

$$I^{SW}(\mathbf{r}) = |E_0|^2 \left[1 + \left|\frac{E_h}{E_0}\right|^2 + 2C\left|\frac{E_h}{E_0}\right| \cos(v + \mathbf{h}\cdot\mathbf{r})\right], \tag{11.10}$$

where v is the phase of the complex amplitude ratio $E_h/E_0 = |E_h/E_0| \times \exp(iv)$ of the X-ray field and C is the polarization coefficient which is equal to one for σ-polarization and $\cos 2\theta$ for π-polarization and 2θ is the angle enclosed by the two wave vectors $\mathbf{k_0}$ and $\mathbf{k_h}$ (see Fig. 11.2).

In case the dipole approximation is valid, the emission signal, Y^h_{Aj}, from any atom of type A within the range of the XSW is proportional to the intensity of the standing wave field at the atom position (11.10) multiplied by the subshell cross-section of the corresponding atom. The superscript h indicates the used diffraction vector $\mathbf{h}$ and subscript j indicates an individual atom of type A. The resulting yield Y^h_T of a large number of atoms is simply the sum of the contributions of the individual atoms, i.e., after normalization

$$Y^h_{AT} = (1/N)\sum_{j=1}^{N} Y^h_{Aj} = 1 + R + 2C\sqrt{R}F^h \cos(v - 2\pi P^h). \tag{11.11}$$

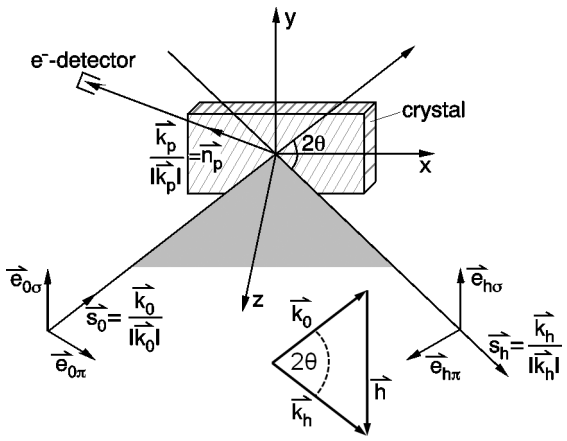

Fig. 11.2. Geometric relationships for the PE process caused by two coherent electromagnetic waves $\mathbf{E_0}$ and $\mathbf{E_h}$ characterized by the wave vectors $\mathbf{k_0}$ and $\mathbf{k_h}$, respectively. The polarization directions are indicated by the vectors $\mathbf{e_{0\sigma}}$, $\mathbf{e_{0\pi}}$, and $\mathbf{e_{h\sigma}}$, $\mathbf{e_{h\pi}}$. The angle 2θ is the angle between the wave vectors $\mathbf{k_0}$ and $\mathbf{k_h}$. The direction of the escaping photoelectron is determined by the vector $\mathbf{k_p}$. The relationship of the vectors $\mathbf{k_o}, \mathbf{k_h}$, and $\mathbf{h}$ is indicated.

In Eq. (11.11), $R = |E_H|^2/|E_0|^2$. The amplitude F^h and the phase factor P^h of the cosine function, the coherent fraction[d] and coherent position, respectively, represent the amplitude and phase of the Fourier coefficients of the distribution function of atoms A. They are determined by a fit to the experimentally recorded yield Y^h_{AT}.[e] This approach works well for the fluorescence yield and the integral photoelectron yield when non-dipole contributions do not exceed a few percent. However, the functional form is not valid any longer when X-ray excited photoelectrons are recorded angularly resolved. Because of higher-order multipole contributions, the emission will be no longer symmetric with respect to the polarization vector, but enhanced in $\mathbf{k}$ or $-\mathbf{k}$ direction. Consequently, the photoelectron signal emitted by two X-ray waves in a specific direction is not the same for both

[d]The coherent fraction is usually written as the product $F^h = A_G(1-U)D^d_h D^s_h$, where A_G is the "geometrical structure factor," U is the uncoherent (randomly distributed fraction), D^d_h is the dynamic (i.e., temperature) Debye–Waller factor, and D^s_h is a static Debye–Waller factor.[6]

[e]For atoms within the bulk of the crystal the functional form of Eq. (11.11) has to be modified because of the extinction of the wave field with increasing depth in the crystal (see Ref. 7 and Chapter 1.10).

waves, even if their polarization vectors are collinear and they have the same strength.

Next, we assume that an atom is present within the range of the XIF and we consider the photoelectric process excited by the XIF. In this case, the coordinate $\mathbf{r}$ of an electron involved in the photoelectron process can be described as $\mathbf{r} = \mathbf{r_a} + \mathbf{r}_e^a$, where $\mathbf{r_a}$ is the position of the center of the atom (in the unit cell, or on the surface) and $\mathbf{r}_e^a$ is the coordinate of this electron with respect to the center of the atom. In case of the superposition of two coherent waves, to obtain the resulting cross section for the photoelectron process, we have to substitute Eq. (11.9) into Eqs. (11.2) and (11.3). The matrix element of the whole process is the sum of the complex matrix elements corresponding to each wave E_0 and E_h,

$$M_{fi} = E_0\langle f|e^{i\mathbf{k_0}\cdot\mathbf{r}_e^a}(\mathbf{e_0}\cdot\hat{\mathbf{p}})|i\rangle + E_h\langle f|e^{i\mathbf{k_h}\cdot\mathbf{r}_e^a}(\mathbf{e_h}\cdot\hat{\mathbf{p}})|i\rangle, \tag{11.12}$$

or

$$M_{fi} = E_0\exp(i\mathbf{k_0}\cdot\mathbf{r_a})\left[M_{fi}(\mathbf{s_0}) + \left(\frac{E_h}{E_0}\right)e^{i\mathbf{h}\cdot\mathbf{r_a}}M_{fi}(\mathbf{s_h})\right], \tag{11.13}$$

where $\mathbf{s_0} = \mathbf{k_0}/|\mathbf{k_0}|$, $\mathbf{s_h} = \mathbf{k_h}/|\mathbf{k_h}|$, and

$$\begin{aligned} M_{fi}(\mathbf{s_0}) &= \langle f|\exp(i\mathbf{k_0}\mathbf{r}_e^a)(\mathbf{e_0}\hat{\mathbf{p}})|i\rangle, \\ M_{fi}(\mathbf{s_h}) &= \langle f|\exp(i\mathbf{k_h}\mathbf{r}_e^a)(\mathbf{e_h}\hat{\mathbf{p}})|i\rangle \end{aligned} \tag{11.14}$$

are the corresponding matrix elements.

The cross-section of the process and hence the intensity of the photoelectron yield $Y(\Omega)$ is proportional to the square modulus of the matrix element given by Eq. (11.13) For each (linear) polarization state we can write,

$$Y(\Omega) \propto d\sigma/d\Omega \propto |M_{fi}|^2,$$

where

$$|M_{fi}|^2 = |E_0|^2\{S_{00} + S_{hh}R + 2\sqrt{R}\ \mathrm{Re}[S_{0h}e^{i(v+\mathbf{hr_a})}]\}. \tag{11.15}$$

Here

$$S_{00} = |M_{fi}(\mathbf{s_0})|^2, \quad S_{hh} = |M_{fi}(\mathbf{s_h})|^2, \quad S_{0h} = M_{fi}(\mathbf{s_0})^* M_{fi}(\mathbf{s_h}). \tag{11.16}$$

The parameters $S_{\alpha\beta}$ (11.16) are, in fact, proportional to the cross-sections of the photoelectron process for the direct, scattered, and interfering beams. By definition, S_{00} and S_{hh} are real numbers and their

values can be calculated as given by Eq. (11.8) with the proper polarization and propagation vectors of the incident and diffracted X-ray waves. However, S_{0h} in general may be complex and can give rise to an additional phase shift $\psi = \arg[S_{0h}/S_{00}]$ for the interference term in (11.15).

Equation (11.15) represents a *general form* for the photoelectron yield function for an atom in an XSW field, which is also valid when non-dipole contributions to the photo-effect are significant. In the case that we are recording the yield from a distribution of atoms on the surface of a crystal we obtain after normalization the *generalized yield function*

$$Y_T^h(\Omega) = 1 + S_R R + 2|S_I|\sqrt{R}F^h \cos(v - 2\pi P^h + \psi), \tag{11.17}$$

where we have introduced new parameters

$$S_R = \frac{S_{hh}}{S_{00}}, \quad S_I = |S_I|e^{i\psi} = \frac{S_{0h}}{S_{00}}. \tag{11.18}$$

The results of an XSW experiment, in which the yield of high-energy photoelectrons is measured, in general, has to be fitted to Eq. (11.17) rather than to Eq. (11.11). Thus, in order to determine accurately the structural parameters coherent fraction and coherent position, knowledge of the parameters $S_R, |S_I|$, and ψ is needed. Below we will concentrate on how this can be done for some specific cases and geometries.

In the case of non-dipole contributions performing the multipole expansion for both matrix elements in (11.15), similar to the case of a single electromagnetic wave (11.4), we get

$$M_{fi}(\mathbf{s_0}) \simeq M_{fi}^D + M_{fi}^Q(\mathbf{s_0}), \quad M_{fi}(\mathbf{s_h}) \simeq M_{fi}^D + M_{fi}^Q(\mathbf{s_h}). \tag{11.19}$$

Only the second term corresponding to quadrupole transitions depends on the propagation vectors $\mathbf{s_0}, \mathbf{s_h}$ but both terms are, in general, complex numbers and can interfere with each other. Equation (11.15) takes into account the interference of the multipole matrix elements M_{fi}^D and M_{fi}^Q (11.19) in addition to the interference of the two coherent X-ray waves E_0 and E_h.

11.4. Matrix Elements for Multipole Terms: General Expression

From our previous analysis, it is clear that the problem of calculating the effect of multipole contributions to the photoelectron yield is reduced to calculating the matrix elements $M_{fi}(\mathbf{s_0})$ and $M_{fi}(\mathbf{s_h})$ for the two coherent

waves. For excitation by *two* coherent waves we are dealing with five different vectors ($\mathbf{k_0}, \mathbf{k_h}, \mathbf{e_0}, \mathbf{e_h}, \mathbf{n_p}$) involved in the process that have to be taken into account simultaneously (see Fig. 11.2) for the following calculation of the matrix elements. For the general formalism of multipole expansion used here, it is not necessary to adopt a specific reference system.

Decomposing the plane electromagnetic wave into multipole fields (see for details in Ref. 26) one obtains (in the non-relativistic limit) for the matrix element of the absorption of a photon with the polarization $\mathbf{e_s}$ the following expression,[f]

$$M_{fi}(\mathbf{s}) = \sum_{LM} B_L Q_{LM}(\mathbf{e_s}\mathbf{Y}^{(e)*}_{LM}(\mathbf{s})), \tag{11.20}$$

where $B_L = -4\pi i^L\sqrt{(2L+1)(L+1)/L}k^L/(2L+1)!!$ and $\mathbf{Y}^{(e)}_{LM}(\mathbf{s})$ are vector spherical harmonics for an EL transition. The quantity

$$Q_{LM} = \frac{e_0}{\sqrt{2L+1}}\langle f|r^L Y_{LM}(\mathbf{n})|i\rangle \tag{11.21}$$

gives us the electric multipole moment of the transition. Here $r = |\mathbf{r}|$ and the unit vector $\mathbf{n} = \mathbf{r}/r$ define the position of the electron within the atom.

Each term in (11.20) represents the absorption of a photon in an electric state with a definite value of the angular momentum L, magnetic moment M, and parity $P = (-1)^L$ and thus gives rise to a 2^L-pole electric (EL) transition: $L = 1$ correspond to dipole ($E1$) transition, $L = 2$ to quadrupole ($E2$), $L = 3$ to octupole ($E3$) and etc.

The initial (bound) state of the particular electron of an atom may be represented by

$$|i\rangle = R_{nl}(r)|lm\rangle = R_{nl}(r)Y_{lm}(\mathbf{n}), \tag{11.22}$$

where $R_{nl}(r)$ is the radial part of the wave function, which can be obtained, in the non-relativistic limit from the Schrödinger equation. In the final (continuum) state, the ejected electron can be described by a plane wave plus an incoming spherical wave[27] by the following expression

$$|f\rangle = \sum_{lm} a_{lm}R_{k_pl}(r)|lm\rangle = \sum_{lm} a_{lm}R_{k_pl}(r)Y_{lm}(\mathbf{n}), \tag{11.23}$$

where $a_{lm} = a_l Y^*_{lm}(\mathbf{n_p}) = (2\pi/k_p)(i)^l \exp(-i\delta_l)Y^*_{lm}(\mathbf{n_p})$. In Eq. (11.23) $R_{k_pl}(r)$ is the radial wave function for the continuous spectrum, normalized

[f]For convenience[26] we are using $\hbar = c = 1$.

by the condition $\int_0^\infty R_{k'_p l}(r) R_{k_p l}(r) r^2 dr = 2\pi\delta(k'_p - k_p)$ and having the asymptotic form[27] for $r \to \infty$

$$R_{k_p l}(r) \sim \frac{2}{r} \sin\left(k_p r - \frac{\pi l}{2} + \delta_l\right). \tag{11.24}$$

Each of the outgoing partial waves of the electron characterized by the angular momentum quantum number l experiences a phase shift δ_l, which is directly related to the form of the scattering potential of the bound electron. It is an important parameter in the theoretical description of the scattering process (see, for e.g., Ref. 27). According to (11.24) the asymptotic (for $r \to \infty$) behavior of the lth partial wave of the emitted electron is determined by δ_l. Corresponding theoretical values of the phase shifts δ_l are available from the NIST data base.[28]

Using Eqs. (11.22)–(11.24) we obtain for the electric multipole moment of the transition (11.21),

$$Q_{LM} = \frac{e_0}{\sqrt{2L+1}} \sum_{l'm'} a^*_{l'm'} \rho^L_{l'} \langle l'm' | Y_{LM}(\mathbf{n}) | lm \rangle, \tag{11.25}$$

where

$$\rho^L_{l'} = \int_0^\infty R_{k_p l'}(r) r^L R_{nl}(r) r^2 dr \tag{11.26}$$

is the radial integral for the 2^L-pole electric transition and the matrix elements $\langle l'm' | Y_{LM}(\mathbf{n}) | lm \rangle$ determine the *transition rules* for the 2^L-pole transitions.

The matrix elements M_{fi} needed for the parameters $S_{\alpha\beta}$ in Eq. (11.16) are now defined by Eqs. (11.20) and (11.21) and (11.25) and (11.26) to *any multipole order*. However, the product of the matrix elements (11.20) contains not only "pure" terms that correspond to dipole–dipole ($E1$–$E1$), quadrupole–quadrupole ($E2$–$E2$), etc. transitions, but also cross terms, especially dipole–quadrupole ($E1$–$E2$) transitions. For the case of the angular-resolved photoelectric process, these are mainly responsible for non-vanishing multipole contributions to the differential cross-section.[1,2]

11.5. Integral Photoelectron Emission from an Interference Field

The total yield of the photoelectrons, Auger electrons, or fluorescence photons emitted from an atom in an XIF is determined by Eqs. (11.15) and (11.17) integrated over all the directions of the escaping photoelectron $\mathbf{n_p}$.

The integration essentially simplifies the solution. Integrating the product of the matrix elements (11.20) $M_{fi}(\mathbf{s}_\alpha)^* M_{fi}(\mathbf{s}_\beta)$ over the whole spatial angle Ω and averaging the result over all the initial magnetic states m yields the following expression[9]

$$\int \langle M_{fi}(\mathbf{s}_\alpha)^* M_{fi}(\mathbf{s}_\beta)\rangle d\Omega \propto \sum_L \sigma^L p_L(\alpha,\beta), \tag{11.27}$$

where indices $\alpha,\beta = 0,h$. In Eq. (11.27), the coefficients σ^L are the total cross-sections of the photoelectron excitation from the subshell n,l corresponding to different multipole transition terms

$$\sigma^L = \frac{A_L}{2l+1}\sum_{l'} |a_{l'}|^2 (\rho^L_{l'})^2 (l'||Y_L||l)^2. \tag{11.28}$$

The coefficients $p_L(\alpha,\beta)$ in (11.27) determine the *angular dependence* on the polarization vectors $\mathbf{e}_{\alpha\mathbf{s}}, \mathbf{e}_{\beta\mathbf{s}}$

$$p_L(\alpha,\beta) = \frac{8\pi}{2L+1}\sum_M (\mathbf{e}_{\alpha\mathbf{s}}\mathbf{Y}^{(e)}_{L'M'}(\mathbf{s}_\alpha))(\mathbf{e}_{\beta\mathbf{s}}\mathbf{Y}^{(e)*}_{LM}(\mathbf{s}_\beta)), \tag{11.29}$$

where index $s = \sigma,\pi$ denotes σ, or π-polarization (see Fig. 11.2). In (11.28), $(l'||Y_L||l)$ are the reduced matrix elements.[29,30]

Taking for example only dipole transitions into account, only one term with $L = 1$ remains in the sum (11.27). Due to the dipole transition rules $l' = l \pm 1$ one obtains from (11.28) the well-known expression[20] for the dipole cross-section,

$$\sigma^D = \frac{A_1}{2l+1}[(l(\rho^D_{l-1})^2 + (l+1)(\rho^D_{l+1})^2], \tag{11.30}$$

where $\rho^D_{l\pm1} = \int_0^\infty R_{kl\pm1}(r) r R_{nl}(r) r^2 dr$ is the dipole integral ($\rho^D_l \equiv \rho^1_l$) (11.26). In the same way we obtain from (11.28) the total cross-sections for quadrupole, octupole, etc. transitions.

As (11.27) shows, after integration over all angles of the escaping photoelectron and averaging over the initial states only "pure" transitions (dipole, quadrupole, etc.) are contributing to the integral PE yield and there are no mixed terms.

Directly from the relations (11.27)–(11.29) one obtain for the parameters $S_{\alpha\beta}$,

$$S_{\alpha\beta} = \sum_L \sigma^L p_L(\alpha,\beta), \tag{11.31}$$

or more explicitly

$$\begin{aligned} S_{00} &= S_{hh} = \sigma^D + \sigma^Q + \sigma^O + \cdots, \\ S_{0h} &= C^D\sigma^D + C^Q\sigma^Q + C^O\sigma^O + \cdots. \end{aligned} \tag{11.32}$$

Here C^D, C^Q and C^O are polarization coefficients corresponding to each multipole term. They can be calculated from (11.29) and are equal to[9]

$$\begin{aligned} C^D &= p_1(0,h) = \mathbf{e_{0s}e_{hs}}, \\ C^Q &= p_2(0,h) = (\mathbf{e_{0s}e_{hs}})(\mathbf{s_0s_h}) + (\mathbf{e_{0s}s_h})(\mathbf{e_{hs}s_0}), \\ C^O &= p_3(0,h) = 1/4\{5[(\mathbf{e_{0s}e_{hs}})(\mathbf{s_0s_h})^2 \\ &\quad + 2(\mathbf{e_{0s}s_h})(\mathbf{e_{hs}s_0})(\mathbf{s_0s_h})] - (\mathbf{e_{0s}e_{hs}})\}. \end{aligned} \tag{11.33}$$

From expression (11.33) for each (σ- and π-) polarization, explicit angular dependence from the scattering angle θ are obtained, i.e.,

$$\begin{aligned} C^D &= \begin{cases} 1, & \sigma\text{-polarization;} \\ \cos 2\theta, & \pi\text{-polarization.} \end{cases} \\ C^Q &= \begin{cases} \cos 2\theta, & \sigma\text{-polarization;} \\ \cos 4\theta, & \pi\text{-polarization.} \end{cases} \\ C^O &= \begin{cases} 1/8[5\cos 4\theta + 3], & \sigma\text{-polarization;} \\ 1/16[15\cos 6\theta + \cos 2\theta], & \pi\text{-polarization.} \end{cases} \end{aligned} \tag{11.34}$$

For the normalized integral intensity of the photoelectron yield from an atom within the XIF according to Eq. (11.17) one, finally, obtains (in this case $S_R = 1$),

$$Y_A^h = 1 + R + 2\tilde{C}\sqrt{R}\cos(v + \mathbf{h}\cdot\mathbf{r_a}), \quad \psi \equiv 0, \tag{11.35}$$

where

$$\tilde{C} \equiv |S_I| = \frac{C^D\sigma^D + C^Q\sigma^Q + C^O\sigma^O + \cdots}{\sigma^D + \sigma^Q + \sigma^O + \cdots}. \tag{11.36}$$

For most applications the contribution from the octupole term can be neglected (see for e.g., calculations in Refs. 31 and 32). In this case we

obtain for the coefficient $\tilde{C}$,

$$\tilde{C} = C^D(1 - Q), \tag{11.37}$$

where the quadrupole contribution is given by

$$Q = (\sigma^Q/\sigma)[1 - C^Q/C^D], \tag{11.38}$$

and $\sigma = \sigma^D + \sigma^Q$ is the total cross-section. For the two polarization states, Eqs. (11.34) yield,

$$Q = \begin{cases} 2(\sigma^Q/\sigma)\sin^2\theta, & \sigma\text{-polarization;} \\ (\sigma^Q/\sigma)\,[\cos 2\theta - \cos 4\theta]\cos 2\theta, & \pi\text{-polarization.} \end{cases} \tag{11.39}$$

So far, there are already two important conclusions. First, in the case of the integral photoelectron yield, according to (11.33), the parameters $S_{\alpha\beta}$ are real numbers. Since $S_{00} = S_{hh}$, additional multipole terms change only the amplitude of the third, the interference term in Eq. (11.35) and multipole contribution can be expressed by one parameter $\tilde{C}$. Second, only in the dipole approximation when ($\sigma^Q = \sigma^O = \cdots = 0$) the photoelectron yield intensity Y_A^h (11.35) features exactly the X-ray wave field intensity (XSW) (11.10) at the particular chosen location in space. Every multipole term in Eq. (11.36) exhibits in fact its own dependence on the scattering angle θ (compare with Ref. 31). This angular dependence allows in principle to determine the multipole terms directly from an XSW experiment.

Interesting results are obtained when analyzing the contribution of the quadrupole term for different scattering angles. For example, an X-ray wave diffracted with a Bragg angle of $\theta = 45°$ is usually regarded as "purely" σ-polarized. However, if quadrupole contributions are taken into account, a "weak" diffracted beam is observed for π-polarization as well. In this case we can obtain from Eq. (11.39): $\tilde{C} = -(\sigma^Q/\sigma)$. Thus, in the case of diffraction for $\theta = 45°$ the interference term in Eq. (11.35) is directly proportional to the value (σ^Q/σ). However, since the reflectivity is (extremely) small in this case, this effect will be difficult to observe.

In the case of the *back reflection*, i.e., for a Bragg angle of $\theta = 90°$ we get from (11.39): $\tilde{C} = 1 - 2(\sigma^Q/\sigma)$ and thus the influence of the quadrupole term is at *maximum*.

In summary, quadrupole terms in the integral cross-section influence the *amplitude* of the cosine function in Eq. (11.35). Thus, the integral photoelectron, Auger electrons, or fluorescence yield depends (due to the different angular dependence of the multipole term) on the value of the

quadrupole contribution (σ^Q/σ) when scanning through the Bragg condition. Equations (11.35) and (11.36) show that the larger the quadrupole contribution the smaller is the coefficient $\tilde{C}$ and hence the smaller is the *apparent* value of the coherent fraction extracted from an XSW experiment. Typical examples for the dependence of the parameter $\tilde{C}$ on scattering angle and energy for σ-polarized radiation are presented in Fig. 11.3. It shows that the quadrupole contribution is enhanced for the standing wave formation when $2\theta \approx \pi$, or if the excitation energy E_γ is near to an absorption edge.

11.6. Angular-Resolved Photoelectron Emission in the Dipole Approximation

In the following, expressions for the angular-resolved photoelectron yield in the presence of XIF will be deduced, starting from the dipole approximation. In this case, the general expression (11.20) for the matrix element M^s_{fi} contains only one term with $L = 1$.

The intensity of the photoelectron yield excited by the XIF is determined by Eqs. (11.15), (11.17), and parameters $S_{\alpha\beta}$ defined in (11.16). Evaluating the matrix elements $M_{fi}(\mathbf{s})$ (11.20) in the dipole approximation one obtains for the parameters $S_{\alpha\beta}$,[9]

$$\begin{aligned} S_{00} &= (\sigma^D/4\pi)[1 + \beta P_2(\mathbf{e_{0s}}\mathbf{n_p})], \\ S_{hh} &= (\sigma^D/4\pi)[1 + \beta P_2(\mathbf{e_{hs}}\mathbf{n_p})], \\ S_{0h} &= (\sigma^D/4\pi)[(1 - \beta/2)(\mathbf{e_{0s}}\mathbf{e_{hs}}) + 3/2\beta(\mathbf{e_{0s}}\mathbf{n_p})(\mathbf{e_{hs}}\mathbf{n_p})]. \end{aligned} \tag{11.40}$$

Here σ^D is the dipole cross-section (11.30) and β is the dipole asymmetry parameter (see Eq. (11.7)).

The expressions for the parameter S_{00} and S_{hh} correspond to equation (11.6) for the subshell n, l, for the proper polarization vectors e_{0s} and e_{hs}, respectively, and neglecting terms beyond dipole, i.e., for the case that $\sigma = \sigma_D$ and $\gamma = \delta = 0$.

The obtained result (see Eqs. (11.15) and (11.40)) allow to calculate the angular distribution of the photoelectrons for any initial state of the electron and different polarization states of the interfering X-ray beams. If the parameter β is known (e.g., from Eq. (11.7)), then the angular distribution of the photoelectrons can be deduced from Eqs. (11.15) and (11.40). On the other hand, if β is *unknown*, then it could be determined from a fit to the experimental data using Eqs. (11.15) and (11.40). From

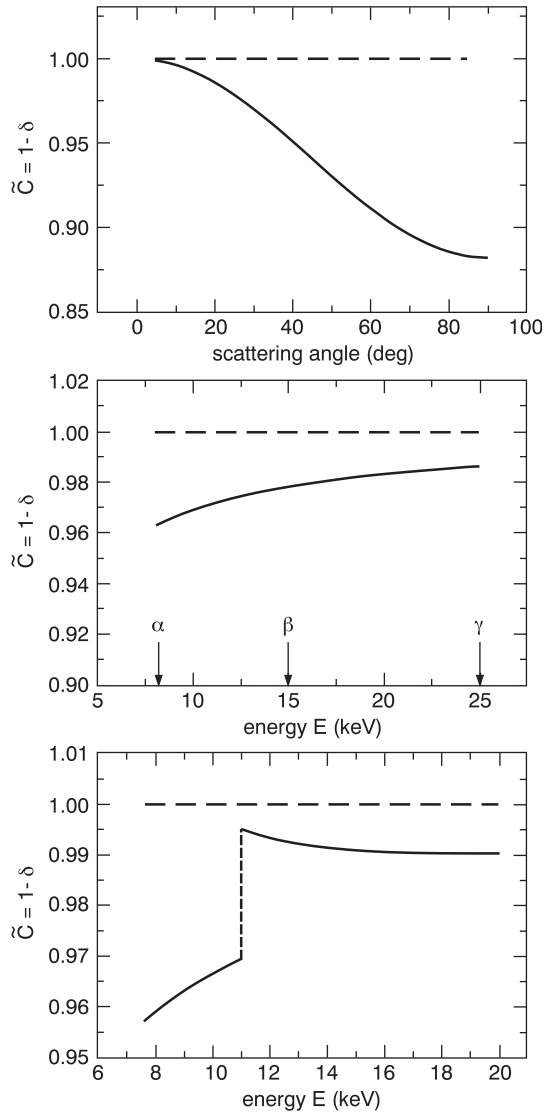

Fig. 11.3. Quadrupole contribution in case of the integral photoelectron yield. For the σ-scattering geometry, $\tilde{C} = 1 - Q$, where $Q = 2(\sigma^Q/\sigma)\sin^2\theta$ as given by Eq. (11.39). (a) $\tilde{C}$ as a function of the scattering angle θ for Si and the photon energy $E_\gamma = 22\,\mathrm{keV}$ ($\sigma^Q/\sigma = 0.059$). (b) $\tilde{C}$ as a function of the photon energy E_γ for a Si (444) reflection. Arrows α, β and γ correspond to the Bragg angles $\theta_B = 81.4°, 31.8°, 18.4°$. (c) $\tilde{C}$ as a function of the photon energy E_γ near the absorption edge of Ge. The quadrupole cross-sections as a function of energy are taken from Ref. 32. The dashed line corresponds to pure dipole case $\tilde{C} = 1$. From Ref. 9

.

Eq. (11.40), we obtain for the parameters S_R and S_I for the normalized photoelectron yield in Eq. (11.17),

$$S_R = \frac{1+\beta c_h}{1+\beta c_0}, \quad |S_I| = \frac{(1-\beta/2)(\mathbf{e_{0s}}\mathbf{e_{hs}})+\beta c_{0h}}{1+\beta c_0}, \quad \psi \equiv 0. \tag{11.41}$$

The parameters c_0=$P_2(\mathbf{e_{0s}}\mathbf{n_p})$, c_h=$P_2(\mathbf{e_{hs}}\mathbf{n_p})$, and c_{0h}=$3/2(\mathbf{e_{0s}}\mathbf{n_p})(\mathbf{e_{hs}}\mathbf{n_p})$ are determined by the geometry of the experiment, in particular, the position of the photoelectron detector.

Naturally, in the dipole approximation, the photoelectron yield does not depend explicitly on the direction of the propagation vectors $\mathbf{s_0}, \mathbf{s_h}$. Moreover, comparing Eqs. (11.15) and (11.40) with the integral photoelectron yield case Eqs. (11.35) and (11.36), we can see that the parameters $S_{\alpha\beta}$ are again real numbers but contrary to the previous case, generally $S_{00} \neq S_{hh} \neq S_{0h}$. As a consequence of this new behavior, for different directions of the photoelectron detector one of the terms in (11.15) can be enhanced or suppressed and in this way *the angular dependence* of the photoelectron yield can be effectively changed while scanning through the interference region of the two beams. For the two different polarizations, σ and π, the influence on the XSW yield curves is drastically different.

In the *σ-polarization* scattering geometry the polarization vectors $\mathbf{e_0}$ and $\mathbf{e_h}$ are collinear (see Fig. 11.2). In this case we obtain for the parameters $S_{\alpha\beta}$ (11.40),

$$S_{00} = S_{hh} = S_{0h} = (\sigma^D/4\pi)[1+\beta P_2(\mathbf{e}_\sigma \mathbf{n_p})]. \tag{11.42}$$

Comparing now this result with the expression (11.10) for the intensity of the standing wave field, we see that in the case of σ-polarization, the photoelectron yield $Y(\Omega)$ has the same functional form as the electric field intensity I^{SW}. For example, in the case of an initial s-state (parameter $\beta = 2$) we get from (11.17) and (11.42) for the photoelectron yield

$$Y_p(\Omega) \propto \cos^2\vartheta_p[1+R+2\sqrt{R}F^h\cos(v-2\pi P^h)]. \tag{11.43}$$

For *π-polarization*, the incident and diffracted electric field vectors lie in the scattering plane and the polarization vectors $\mathbf{e_0}$ and $\mathbf{e_h}$ are misaligned by twice the magnitude of the Bragg-angle 2θ (see Fig. 11.2). Unlike the situation for σ-polarization, the angular momenta of the initial $|i\rangle$ and final $|f\rangle$ state electron wave functions now influence the behavior of $d\sigma/d\Omega$ as the interference condition is fulfilled.

If the initial state has *s angular momentum symmetry*, the final state has p symmetry. In this case the parameter β (11.7) is (to a very good

approximation[22]) equal to $\beta = 2$, and we obtain for the parameters $S_{\alpha\beta}$ (11.40) in (11.15),

$$\begin{aligned} S_{00} &= 3(\sigma^D/4\pi)(\mathbf{e_{0\pi}}\mathbf{n_p})^2 = 3(\sigma^D/4\pi)\cos^2\vartheta_{p0}, \\ S_{hh} &= 3(\sigma^D/4\pi)(\mathbf{e_{h\pi}}\mathbf{n_p})^2 = 3(\sigma^D/4\pi)\cos^2\vartheta_{ph}, \\ S_{0h} &= 3(\sigma^D/4\pi)(\mathbf{e_{0\pi}}\mathbf{n_p})(\mathbf{e_{h\pi}}\mathbf{n_p}) = 3(\sigma^D/4\pi)\cos\vartheta_{p0}\cos\vartheta_{ph}, \end{aligned} \tag{11.44}$$

where ϑ_{p0} and ϑ_{ph} are the polar angles of the emitted electron relative to $\mathbf{e_{0\pi}}$ and $\mathbf{e_{h\pi}}$, respectively (the z-axis is directed along the vector $\mathbf{n_p}$).

The photoelectron yield $Y_p(\Omega)$ (cf. Eq. (11.15)) is now expressed as

$$Y_p(\Omega) \propto \cos^2\vartheta_0 + \cos^2\vartheta_h R + 2\cos\vartheta_0\cos\vartheta_h\sqrt{R}F^h\cos(v - 2\pi P^h). \tag{11.45}$$

If the detector is at a position satisfying the condition: $\vartheta_{p0} \approx 90^\circ$ (in this case $S_{00} \simeq 0$) or $\vartheta_{ph} \approx 90^\circ$ ($S_{hh} \simeq 0$), the influence of either the direct or the scattered beam can effectively be suppressed, as is obvious from Eq. (11.45). This will drastically change the photoelectron yield curve. Experimental results[8] of the L_I photoelectron yield from iodine adsorbed on a Ge(111) single crystal as a function of glancing angle in the vicinity of the (111) germanium reflection are reproduced in Fig. 11.4. Shown are the results for two different emission angles of the photoelectrons. The solid lines are fits to the data according to Eq. (11.45).

When the initial electron state has *p angular momentum symmetry* ($l = 1$), dipole selection rules allow transitions to continuum states with pure s and pure d character, as well as states with mixed $s-d$ character. The latter arise from interference of the outgoing s and d photoelectron waves.[33] In this case one obtains for the "asymmetry parameter" β from (11.7),

$$\beta = \frac{2\rho[\rho - 2\cos(\delta_d - \delta_s)]}{1 + 2\rho^2}, \tag{11.46}$$

where $\rho = \rho_d^D/\rho_s^D$. Thus, in this case two competing outgoing channels are always present, and consequently the photoelectron yield (11.15) (with parameters $S_{\alpha\beta}$ determined in (11.40) and β from Eq. (11.46)) will depend on the interference between the s and d partial waves. This, in turn, is most sensitive to the phase shift difference $\delta_d - \delta_s$, although it also depends on the relative magnitudes of the dipole integrals ρ_s^D and ρ_d^D. The angular dependence of the photoelectron yield in the particular case of "pure" $p \to s$ or $p \to d$ transitions was considered in detail earlier.[9]

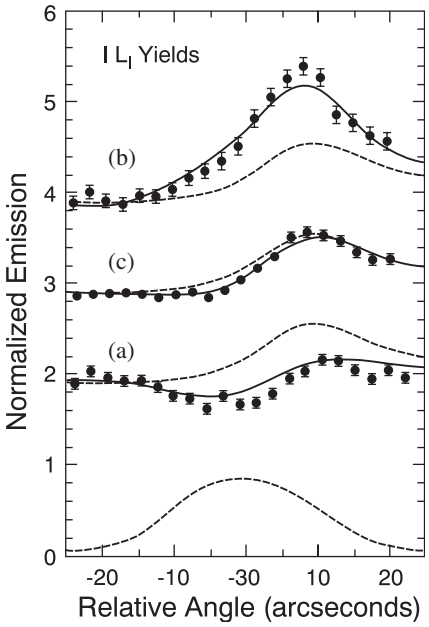

Fig. 11.4. The iodine L_I photoelectron (kinetic energy 1560 eV) yield as a function of glancing angle around the maximum reflectivity of the Ge(111) Bragg reflection for a π-scattering geometry, recorded with different adjustments of the CMA angular aperture: for curve (a), the aperture selects photoelectrons emitted almost in the direction of the polarization vector of the incident beam; for curve (b), the aperture is adjusted to select photoelectrons emitted almost in the direction of the polarization vector of the reflected beam; for curve (c), the aperture was removed, and a wider range of emission angles was selected. The lowest curve is the Ge(111) reflectivity. The theoretical yields shown as solid curves assume an $s \rightarrow p$ dipole transition (cf. Eq. (11.45)); the dashed curves follow the electric field intensity (Eq. (11.10)), i.e., their functional form is given by Eq. (11.17) with $S_R = |S_I| = 1$ and $\psi = 0$. From Ref. 8.

This analysis shows that the shape of the angular-resolved photoelectron yield curves expected from an XSW experiment in the dipole approximation is, in fact, determined by the value of the "asymmetry" parameter β. This value can be different for different subshells and for a given subshell it varies with the photon energy.

11.7. Angular-Resolved Photoelectron Emission in the Dipole–Quadrupole Approximation

As next, the angular distribution of the photoelectron yield from an atom in the XIF is considered, when in addition to the dipole term the quadrupole

term has to be taken into account. It is assumed in the following that the initial state of the electron in the atom is an *s-state*, before considering the practically important case of an initial *p-state* of the photoelectron.

11.7.1. *s-initial state*

The photoelectron yield $Y(\Omega)$ (11.15) from an atom in the XSW field is determined by the matrix element defined by Eq. (11.20). Considering dipole ($s \to p$) and quadrupole ($s \to d$) transitions, after straightforward calculations[9] we obtain for the parameters $S_{\alpha\beta}$ in Eq. (11.16)

$$\begin{aligned} S_{00} &= 3(\sigma^D/4\pi)(\mathbf{e_0 n_p})^2[1+\gamma'(\mathbf{s_0 n_p})], \\ S_{hh} &= 3(\sigma^D/4\pi)(\mathbf{e_h n_p})^2[1+\gamma'(\mathbf{s_h n_p})], \\ S_{0h} &= 3(\sigma^D/4\pi)(\mathbf{e_0 n_p})(\mathbf{e_h n_p})\left\{1+\frac{1}{2}[\widetilde{\gamma}^*(\mathbf{s_0 n_p})+\widetilde{\gamma}(\mathbf{s_h n_p})]\right\}. \end{aligned} \tag{11.47}$$

The complex parameter $\widetilde{\gamma}$ is defined as

$$\widetilde{\gamma} = \gamma' + i\gamma'' = \gamma_0 e^{i\Delta}, \quad \gamma_0 = k\frac{\rho_d^Q}{\rho_p^D}, \quad \Delta = \delta_d - \delta_p. \tag{11.48}$$

It is determined by the values of the dipole $\rho_p^D = \int_0^\infty R_{k_p l'=1}(r) r^3 \times R_{nl=0}(r) dr$ and quadrupole $\rho_d^Q = \int_0^\infty R_{k_p l'=2}(r) r^4 R_{nl=0}(r) dr$ integrals (11.26) and the partial phase shifts δ_p, δ_d of the final electron p- and d-state (see Eq. (11.24)). In the case of a single propagating wave, the obtained results are reduced to the ones described by Eq. (11.8) with the parameter γ defined as $\gamma = 3\gamma'$. Furthermore, for a pure dipole transition $\widetilde{\gamma} = 0$.

In case of quadrupole contributions to the photoelectron yield excited by an interference field, generally $S_{00} \neq S_{hh} \neq S_{0h}$. The parameter S_{0h} is now a *complex* number with amplitude and *phase* depending on the photon energy and the scattering geometry. The phase ψ in the expression for the photoelectron yield (11.17) appears only for the angular-resolved PE when the quadrupole term in the multipole expansion is taken into account and it vanishes in the integral PE case (see Sec. 4).

For *σ-polarization* and the particular geometry of the experiment shown in Fig. 11.2, the expressions (11.47) are further simplified. Assuming that the photoelectron detector is located in the (z, y) plane we obtain,[9]

$$S_R = S_{00}/S_{hh} = \frac{1+\gamma'(\mathbf{s_0 n_p})}{1+\gamma'(\mathbf{s_h n_p})} = \frac{1+C_p\gamma'}{1-C_p\gamma'}, \quad S_I = \frac{1+iC_p\gamma''}{(1-C_p\gamma')}. \tag{11.49}$$

Here, for the scattering geometry of Fig. 11.2, the parameter C_p has the value $C_p = \cos\theta_p \sin\theta$, where θ_p is the angle between the z-axis and the propagation vector of the photoelectron (we assume that $\theta_p < \pi/2$). In case of a small multipole contribution ($\widetilde{\gamma} \ll 1$) we obtain for the parameters in Eq. (11.49) $S_R \simeq 1 + 2C_p\gamma'$, $|S_I| \simeq 1 + C_p\gamma', \tan\psi \simeq C_p\gamma''$.

In the *normal incidence geometry*, which is used in many XSW experiments, non-dipole contributions are maximized in the photoelectron yield and cannot be neglected. In this case $\mathbf{s_0 n_p} = -\mathbf{s_h n_p}$ and for the parameter C_p in Eq. (11.49), one obtains $C_p = \cos\theta_p$, where θ_p is an angle between the direction of the escaping photoelectron $\mathbf{n}_p$ and the wave vector $\mathbf{k}_h$. For the normalized photoelectron yield $Y_T^h(\Omega)$ the general expression (11.17) will be valid with parameters

$$S_R = \frac{1+Q'}{1-Q'}, \quad S_I = \frac{1+iQ''}{1-Q'}, \tag{11.50}$$

where $Q' = \gamma' \cos\theta_p$ and $Q'' = \gamma'' \cos\theta_p$. The angular distribution of the photoelectron yield $Y(\Omega)$ calculated according to Eq. (11.17) with and without quadrupole contribution and for different positions of the XSW field is presented in Fig. 11.5.

Directly from (11.50) (this is valid also for the conventional Bragg scattering geometry described by Eq. (11.49)), it can be shown that the three non-dipole parameters are not independent. The following relation is valid

$$|S_I| = 0.5(S_R + 1)\sqrt{1 + \tan^2\psi}, \tag{11.51}$$

and two non-dipole parameters only allow to retrieve the structural XSW parameters F^h and P^h (*cf.* Eq. (11.17)).

We will consider now the system composed of an ensemble of atoms absorbed on a crystal surface. The non-dipole parameter S_R can be determined by preparing and measuring an incoherent film, i.e., when $F^h = 0$. In case of an ordered coherent film or a monolayer, when one wants to determine the coherent fraction F^h and the coherent position P^h (*cf.* Eq. (11.17)) the parameter $|S_I|$ and the phase ψ are still unknown. However, taking into account Eq. (11.51), it is sufficient to know either $|S_I|$ or ψ. In the case of an initial s-state we can utilize the relationship between the phase ψ and the partial phase shift $\Delta = \delta_d - \delta_p$ of the electron final p-

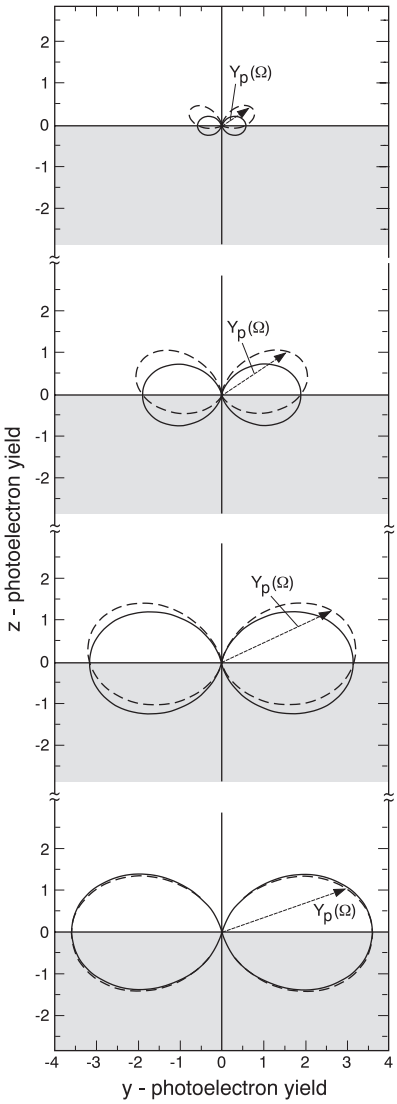

Fig. 11.5. The angular distribution of photoelectrons excited by the XSW field in the backscattering geometry without (solid line) and with (dashed line) quadrupole contribution, according to Eq. (11.17) for different values of the intensity ratio (or reflectivity) $R = |E_H|^2/|E_0|^2$ and phase $\Phi = v - \mathbf{hR_A}$. From top to bottom: $R = 0.95$, $\Phi = -3\pi/4$, $R = 0.9$, $\Phi = -\pi/2$, $R = 0.85$, $\Phi = -\pi/4$, $R = 0.8$, $\Phi = 0$. The beam is polarized in the y-direction and incident on the crystal (shaded region, with the surface at $z = 0$) in $-z$ direction. From Ref. 9.

and d-states. From (11.48) and (11.50) we obtain

$$\tan\psi = \frac{S_R - 1}{S_R + 1}\tan\Delta, \tag{11.52}$$

and applying Eq. (11.51), $|S_I|$ can be determined.

Values of the scattering phase shifts δ_p and δ_d can be obtained from relativistic *ab initio* calculations (see e.g., Ref. 28). These values are needed and used, e.g., in bulk and surface-sensitive structural X-ray methods, which employ electron scattering such as extended X-ray absorption fine structure (EXAFS) and X-ray absorption near edge structure (XANES).[34]

In Figs. 11.6, 11.7 and 11.8, the calculated values of parameters S_R, $|S_I|$ and $\tan\psi$ as a function of the photoelectron energy from 100 to 5000 eV are presented. Different light atoms from carbon to neon are considered. The values of non-dipole parameter S_R were calculated using Eq. (11.50) for $1s$-state of these light atoms. The tabulated values[22] of the parameter γ were used in these calculations. The XSW phase $\tan\psi$ was calculated by expression (11.52) in which the phase shift difference $\Delta = \delta_d - \delta_p$ for each atom and energy was obtained from Ref. 28. The values of parameter $|S_I|$ were determined from Eq. (11.51). In all calculations, the photoelectron escape angle was fixed to the value $\vartheta_p = 45°$. We can see from Fig. 11.8 that the XSW phase ψ contribution can reach the value up to 0.1 rad for light atoms and energies up to 5 keV. For many XSW measurements, the error in determining the phase $2\pi P^h + \psi$ is frequently larger than 0.1 rad. In this case, the contribution of the phase ψ to the XSW photoelectron yield as expressed in Eqs. (11.17) and Eq. (11.51) can frequently be neglected. With this approximation we obtain

$$|S_I| \approx 0.5(S_R + 1). \tag{11.53}$$

For the typical values of $S_R \approx 1.75$ we get for $|S_I| \approx 1.38$, which underlines the importance of these parameters and the necessity of using for the XSW analysis an expression in the form of Eq. (11.17). This approach to determine Δ and consequently the XSW phase ψ was used in Refs. 16 and 35.

It follows from our analysis that non-dipole contributions change the form of the total photoelectron yield curve described by Eq. (11.17). Consequently, if both parameters γ' and γ'' are determined from the experiment, then the values of the dipole and quadrupole integrals and the values of the partial phase shifts δ_p and δ_d for the p- and d-asymptotic

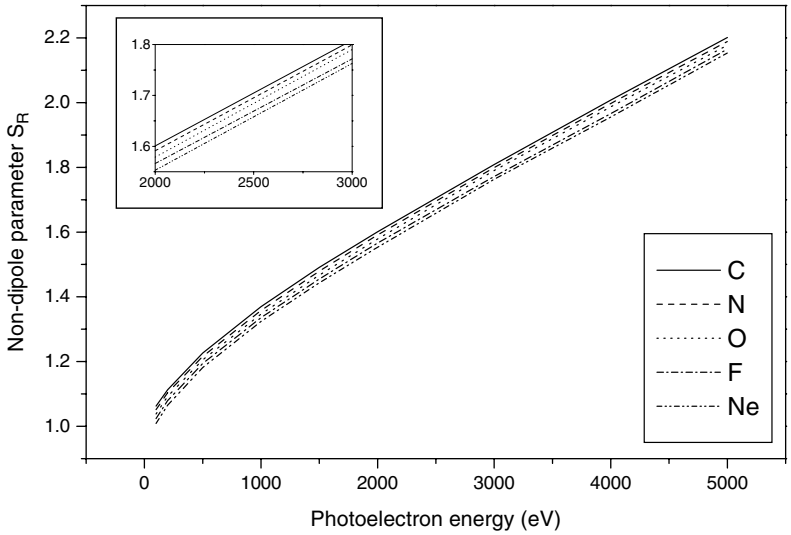

Fig. 11.6. Non-dipole parameter S_R calculated by Eq. (11.50) with parameter γ obtained from the tables.[22] Photoelectron energy range from 2 to 3 keV is shown in the inset.

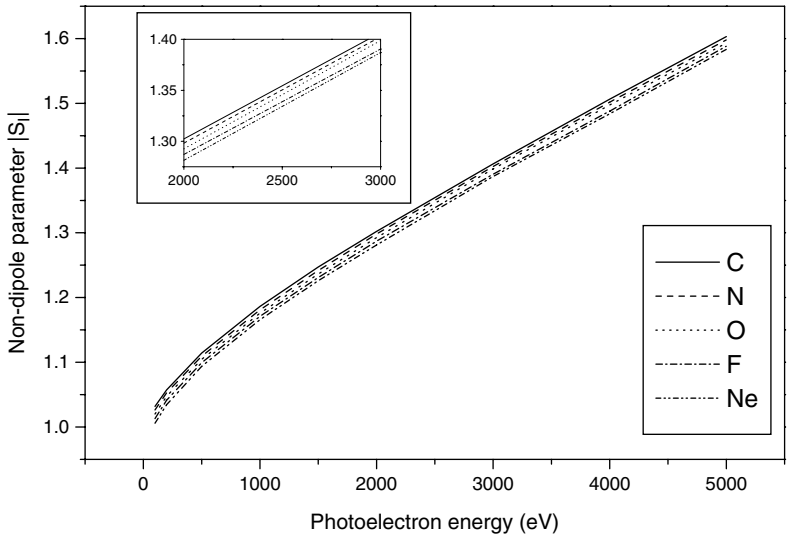

Fig. 11.7. Non-dipole parameter $|S_I|$ calculated according to Eq. (11.51). Photoelectron energy range from 2 to 3 keV is shown in the inset.

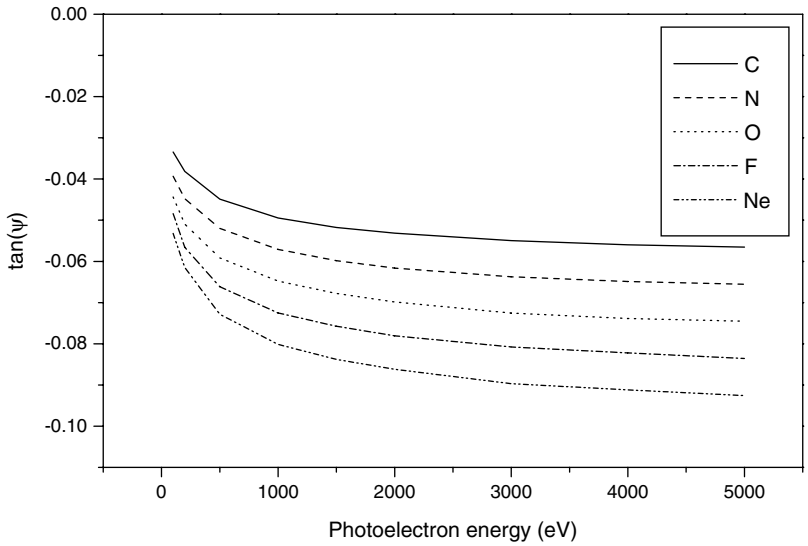

Fig. 11.8. The phase contribution $\tan(\psi)$ calculated by Eq. (11.52). The phase shifts difference $\Delta = \delta_d - \delta_p$ for each atom and energy was obtained by Ref. 28.

wave can be directly extracted. Indeed, inverting Eq. (11.48) we get

$$\rho_d^Q/\rho_p^D = \frac{1}{k}\sqrt{\gamma'^2 + \gamma''^2}, \quad \delta_d - \delta_p = \Delta = \arctan\left[\frac{\gamma''}{\gamma'}\right]. \tag{11.54}$$

By comparing measurements and theoretical predictions for these phase shifts, additional information about the interaction potential of the escaping electron and the residual ion could be obtained.

11.7.2. *p-initial state*

For excitation of initial states of the atom higher than *s*-state, the simple relationship of the multipole parameters S_R, S_I and ψ with the atomic parameters (see Eqs. (11.47) and (11.48)) is no longer valid. However, as shown in Ref. 17, even in these cases, for the backscattering geometry, a parameterization similar to that of the *s*-initial state can be used

$$S_R = \frac{1+Q'}{1-Q'} = \frac{1+q\cos\Delta\phi}{1-q\cos\Delta\phi}, \quad S_I = \frac{1+iQ''}{1-Q'} = \frac{1+iq\sin\Delta\phi}{1-q\cos\Delta\phi}. \tag{11.55}$$

Here $q = 2|M^Q|/|M^D|$ and $\Delta\phi \equiv \phi_q - \phi_d$, where $|M^D|$, $|M^Q|$ and ϕ_d, ϕ_q are the amplitude and phase values of the complex dipole and quadrupole matrix elements $M^D \equiv |M^D|\exp(i\phi_d)$ and $M^Q \equiv |M^Q|\exp(i\phi_q)$.

For the amplitude $|S_I|$ in Eq. (11.55) the same expression as derived in Eq. (11.51) can be applied if the parametrization in the form of Eq. (11.55) is adopted. The relationship

$$\tan\psi = \frac{S_R - 1}{S_R + 1}\tan\Delta\phi \tag{11.56}$$

between XSW phase ψ and the phase difference $\Delta\phi$ will be also valid. If the non-dipole parameters q and $\Delta\phi$ are determined by experiment, the value of the non-dipole contribution parameter Q' in (11.55) can be compared with theoretical values. Using Eq. (11.6) we have for the non-dipole term

$$Q' = \frac{(\delta + \gamma\sin^2\theta_p)\cos\theta_p}{1 + \beta P_2(\sin\theta_p)}, \tag{11.57}$$

where θ_p is the angle for the photoelectron escape.

In experiment,[17] a single-crystal Ge was used as a sample and the parameters q and $\Delta\phi$ were obtained by fitting experimental XSW angular dependence[g] to Eqs. (11.17) and (11.55). Coherent fraction F^h and coherent position P^h were determined by fitting the integral PE yield, which is quite insensitive to non-dipole effects, to Eq. (11.11). The analysis yielded for the parameters $Q'^{\exp}_{3d} = 0.219 \pm 0.07$ and $Q'^{\exp}_{3p} = 0.151 \pm 0.17$. The same parameters calculated by Eq. (11.57) and β, γ, and δ from the Ref. 22 gives $Q'^{th}_{3d} = 0.226$ and $Q'^{th}_{3p} = 0.099$, which is in a good agreement with experimental results.

11.8. Theory of Valence-Electron Emission by an X-Ray Standing Wave

We turn our attention now to PE from the valence band of a single crystal. Because the valence electrons are delocalized, we must consider the emission from all of the atoms within the crystalline unit cell, rather than from a single type of atom as is typically assumed for standard XSW analysis. Furthermore, we assume that we do not energy discriminate between valence states of different energy. For simplicity, we assume that our unit cell has two atoms, and we label these atoms as a for the anion sites and c for the cation sites, respectively. The initial bound-state wave

[g]The same expression for the angular-resolved photoelectron yield in the form of Eq. (11.17) will be valid for crystalline sample if the photoelectron escape depth L_{yi} is much smaller then the extinction depth L_{ex} of the X-ray field in crystal (see for details Ref. 7).

function of a valence electron can be taken in the tight-binding, bond-orbital approximation[36,37] as the sum of the hybridized valence atomic orbitals on each of the cores. As a Bloch wave, our initial-state wave function may therefore be written

$$|i\rangle = \sum_{\mathbf{R}_n} e^{i\mathbf{k}\cdot\mathbf{R}_n}[u_a\phi_a(\mathbf{r}-\mathbf{r}_a-\mathbf{R}_n)+u_c\phi_c(\mathbf{r}-\mathbf{r}_c-\mathbf{R}_n)]. \tag{11.58}$$

Here $\phi_a(\mathbf{r})$ and $\phi_c(\mathbf{r})$ are the hybrid, atomic state valence orbitals of atom a and atom c. For the III–V semiconductors, these are the hybridized s–p states. Coefficients u_a and u_c are defined in terms of the bond polarity α_p, which is calculated from the Hartree–Fock term values of the free atoms[36]

$$u_a = \sqrt{(1+\alpha_p)/2}, \quad u_c = \sqrt{(1-\alpha_p)/2}. \tag{11.59}$$

The coordinate vectors $\mathbf{R}_n$ describe the positions of the unit cells and $\mathbf{r}_a$ and $\mathbf{r}_c$ are the positions of the anion and the cation atoms within each unit cell. For the (111) reflection of the group III–V semiconductors, $\mathbf{r}_c - \mathbf{r}_a = 0.25a[111]$, where a is the lattice parameter.

Since typical XSW experiments are performed at several keV photon energy, we may use the Born approximation[38] that describes the final-state wave function of the escaping photoelectron as a plane wave traveling with the wave vector $\mathbf{k}_f$

$$|f\rangle = e^{i\mathbf{k}_f\cdot\mathbf{r}}. \tag{11.60}$$

According to our general approach formulated in Secs. 11.2 and 11.3 in order to calculate the cross-section of the photoelectron effect in the presence of the XSW field, we must first calculate the differential cross-section using the total electric field from Eq. (11.9). The intensity of the photoexcitation process is proportional to the square modulus of the transition-matrix element M_{fi} (see Eq. (11.2)) between the initial and final states given by Eqs. (11.58) and (11.60). According to Eq. (11.13) the matrix element of the photoelectron process is the sum of the matrix elements corresponding to the direct and diffracted waves

$$M_{fi} = E_0 M_{fi}(\mathbf{s}_0) + E_h M_{fi}(\mathbf{s}_h), \tag{11.61}$$

where matrix elements for the direct $M_{fi}(\mathbf{s}_0)$ and diffracted $M_{fi}(\mathbf{s}_h)$ waves are defined in the Eq. (11.15).

We will now calculate each matrix element separately. Using Eqs. (11.58) and (11.60) for our initial- and final-state wave functions, and performing the change of variables to electron coordinates $\mathbf{r}_e^a = \mathbf{r} - \mathbf{r}_a - \mathbf{R}_n$

and $\mathbf{r}_e^c = \mathbf{r} - \mathbf{r}_c - \mathbf{R}_n$ in each anion and cation term, we arrive at an expression for $M_{fi}(\mathbf{s_0})$

$$M_{fi}(\mathbf{s_0}) = \sum_{\mathbf{R}_n} e^{i(\mathbf{k}+\mathbf{k}_0-\mathbf{k}_f)\cdot\mathbf{R}_n} \cdot [u_a e^{i(\mathbf{k}_0-\mathbf{k}_f)\cdot\mathbf{r}_a} \langle f|e^{i\mathbf{k_0}\cdot\mathbf{r}_e^a}(\mathbf{e_0}\widehat{\mathbf{p}})|\phi_a\rangle + u_c e^{i(\mathbf{k}_0-\mathbf{k}_f)\cdot\mathbf{r}_c} \langle f|e^{i\mathbf{k_0}\cdot\mathbf{r}_e^c}(\mathbf{e_0}\widehat{\mathbf{p}})|\phi_c\rangle]. \quad (11.62)$$

Performing the sum in Eq. (11.62) over the coordinates $\mathbf{R}_n$ of the unit cells, we obtain the conservation law of quasi-momentum for the photoelectron process $\sum_{\mathbf{R}_n} e^{i(\mathbf{k}+\mathbf{k}_0-\mathbf{k}_f)\mathbf{R}_n} = N \cdot \delta_{\mathbf{k}_f,\mathbf{k}+\mathbf{k}_0+\mathbf{g}}$, where N is the number of unit cells, δ is the Kronecker delta, and $\mathbf{g}$ is a reciprocal-lattice vector.[37] Finally, we obtain an expression for the matrix element $M_{fi}(\mathbf{s_0})$

$$M_{fi}(\mathbf{s_0}) \propto [u_a e^{i(\mathbf{k}_0-\mathbf{k}_f)\cdot\mathbf{r}_a} V_a(\mathbf{s_0}) + u_c e^{i(\mathbf{k}_0-\mathbf{k}_f)\cdot\mathbf{r}_c} V_c(\mathbf{s_0})], \quad (11.63)$$

where the matrix elements $V_{a,c}(\mathbf{s_0})$

$$V_{a,c}(\mathbf{s_0}) = \langle f|e^{i\mathbf{k_0}\cdot\mathbf{r}_e^{a,c}}(\mathbf{e_0}\cdot\widehat{\mathbf{p}})|\phi_{a,c}\rangle \quad (11.64)$$

correspond to the elementary photoexcitation process from the anion a and cation c sites for the incident beam. Integration in Eq. (11.64) is performed over the electron coordinates $\mathbf{r}_e^a$ and $\mathbf{r}_e^c$, which are the electron-position vectors from the anion and cation sites in each integral, respectively.

Performing the same calculation for the diffracted beam, we obtain for the matrix element $M_{fi}(\mathbf{k_h})$

$$M_{fi}(\mathbf{s_h}) \propto [u_a e^{i(\mathbf{k_h}-\mathbf{k}_f)\cdot\mathbf{r}_a} V_a(\mathbf{s_h}) + u_c e^{i(\mathbf{k_h}-\mathbf{k}_f)\cdot\mathbf{r}_c} V_c(\mathbf{s_h})], \quad (11.65)$$

where we also have

$$V_{a,c}(\mathbf{s_h}) = \langle f|e^{i\mathbf{k_h}\cdot\mathbf{r}_e^{a,c}}(\mathbf{e_h}\cdot\widehat{\mathbf{p}})|\phi_{a,c}\rangle. \quad (11.66)$$

If we now substitute the expressions for the matrix elements of the incident (Eq. (11.63)) and diffracted (Eq. (11.65)) beams into Eq. (11.61), after some algebra we arrive at the most general expression for the transition-matrix element for the photoelectron effect from a crystal-valence band

$$M_{fi} = E_0\{u_a e^{i(\mathbf{k}_0-\mathbf{k}_f)\cdot\mathbf{r}_a}[V_a(\mathbf{s_0}) + (E_h/E_0)e^{i\mathbf{h}\cdot\mathbf{r}_a}V_a(\mathbf{s_h})] + u_c e^{i(\mathbf{k}_0-\mathbf{k}_f)\cdot\mathbf{r}_c}[V_c(\mathbf{s_0}) + (E_h/E_0)e^{i\mathbf{h}\cdot\mathbf{r}_c}V_c(\mathbf{s_h})]\}. \quad (11.67)$$

According to Eq. (11.2), the magnitude squared of this expression gives the differential cross-section for the valence electron emission in the presence

of two coherently coupled X-ray beams

$$\begin{aligned}\frac{d\sigma}{d\Omega} \sim\ & u_a^2|V_a(\mathbf{s_0}) + (E_h/E_0)e^{i\mathbf{h}\cdot\mathbf{r}_a}V_a(\mathbf{s_h})|^2 \\ & + u_c^2|V_c(\mathbf{s_0}) + (E_h/E_0)e^{i\mathbf{h}\cdot\mathbf{r}_c}V_c(\mathbf{s_h})|^2 \\ & + u_a u_c e^{i(\mathbf{k}_0-\mathbf{k}_f)\cdot(\mathbf{r}_c-\mathbf{r}_a)}[V_a(\mathbf{s_0}) + (E_h/E_0)e^{i\mathbf{h}\cdot\mathbf{r}_a}V_a(\mathbf{s_h})]^* \\ & \times [V_c(\mathbf{s_0}) + (E_h/E_0)e^{i\mathbf{h}\cdot\mathbf{r}_c}V_c(\mathbf{s_h})] + c.c. \end{aligned} \tag{11.68}$$

Here, *c.c.* denotes the complex conjugate. Note, that the equation conventionally used in the studies of the X-ray PE from a crystal-valence band from a single propagating electromagnetic beam[39,40] is obtained from Eq. (11.68) by setting $E_h = 0$.

As valence electrons have negligible binding energies ($\varepsilon_b \sim 0$), the product $|(\mathbf{k}_0 - \mathbf{k}_f)\cdot(\mathbf{r}_c - \mathbf{r}_a)|$ will be much greater than 1 at X-ray energies; consequently, the phase factor $e^{i(\mathbf{k}_0-\mathbf{k}_f)\cdot(\mathbf{r}_c-\mathbf{r}_a)}$ will be highly oscillatory, and, therefore, one can neglect the cross-terms compared to the first two terms of Eq. (11.68).[39–41] This approximation leads us to the differential cross-section for two independent mixed-site emitters in the presence of two coherently coupled X-ray beams

$$\begin{aligned}\frac{d\sigma}{d\Omega} \sim\ & u_a^2|V_a(\mathbf{s_0}) + (E_h/E_0)V_a(\mathbf{s_h})|^2 \\ & + u_c^2|V_c(\mathbf{s_0}) + (E_h/E_0)e^{i\mathbf{h}\rho}V_c(\mathbf{s_h})|^2. \end{aligned} \tag{11.69}$$

As we are interested in the integral photoeffect, we will be integrating Eq. (11.69) over all solid angle $d\Omega$. It is also possible to take into account non-dipole contributions to the XSW yield. According to the results obtained in Sec. 11.5 (see Eq. (11.27)), integration of matrix elements in Eq. (11.69) in terms of their dipole and quadrupole contributions is given by

$$\begin{aligned}\int |V_{a,c}(\mathbf{s_{0,h}})|^2 d\Omega &\propto \sigma_{a,c}^D + \sigma_{a,c}^Q, \\ \int V_{a,c}^*(\mathbf{s_0})V_{a,c}(\mathbf{s_h})d\Omega &\propto C^D\sigma_{a,c}^D + C^Q\sigma_{a,c}^Q, \end{aligned} \tag{11.70}$$

where $\sigma_{a,c}^D$ and $\sigma_{a,c}^Q$ are the total dipole and quadrupole cross-sections for the anion and cation atoms, and C^D and C^Q are the dipole and quadrupole polarization parameters defined in Eqs. (11.33) and (11.34). From Eqs. (11.69) and (11.71), we now obtain the intensity of the total

valence-electron emission from the two coherently coupled beams

$$Y_T \sim u_a^2\sigma_a^T[1+R+2C^D(1-Q_a)\sqrt{R}\cos(v+\mathbf{h}\cdot\mathbf{r}_a)] + u_c^2\sigma_c^T[1+R+2C^D(1-Q_c)\sqrt{R}\cos(v+\mathbf{h}\cdot\mathbf{r}_c)], \quad (11.71)$$

where $\sigma_{a,c}^T = \sigma_{a,c}^D + \sigma_{a,c}^Q$, and $Q_{a,c}$ are the quadrupole contributions for the anion and cation sites, respectively (see Eqs. (11.38) and (11.39)). Note that the inclusion of the quadrupole contributions to the integral photoelectron yield breaks the strict proportionality between the electric-field intensities and the valence-electron emissions by reducing the amplitudes or coherent fractions of the XSW modulations. The coherent position will also be affected, but only in cases where Q_a and Q_c are large and differ by a significant amount.

For the total valence band photoelectron yield in the dipole approximation, i.e., if the quadrupole contributions can be neglected ($Q_a = Q_c = 0$), Eq. (11.71) simplifies to

$$Y_T \sim u_a^2\sigma_a^T[1+R+2C^D\sqrt{R}\cos(v+\mathbf{h}\cdot\mathbf{r}_a)] + u_c^2\sigma_c^T[1+R+2C^D\sqrt{R}\cos(v+\mathbf{h}\cdot\mathbf{r}_c)]. \quad (11.72)$$

Comparison with Eq. (11.10) shows that in dipole approximation the valence-electron emission associated with each atom is directly proportional to the electric-field intensity at the location of its electronic core.

Expression (11.71) for the total photoelectron yield can be written in the usual parametrized form of the XSW yield from an ensemble of atoms

$$Y_T = 1 + R + 2C^D\sqrt{R}F^h\cos(v+2\pi P^h), \quad (11.73)$$

where the parameters P^h and F^h are the coherent position and coherent fraction, respectively. Different from core-emission XSW measurements, the photo-emitted electron can originate from different atomic species and elements. Thus, for valence band or conduction band emission P^h and F^h may be described as the phase and amplitude of the hth Fourier coefficient of the $\mathbf{h}$ residence probability function of the valence electrons, weighted, however, by specific cross-sections.

Using a trigonometric identity, Eqs. (11.71) and (11.73) render

$$F^h e^{2\pi i P^h} = \frac{(1-Q_a)u_a^2\sigma_a^T e^{i\mathbf{h}\cdot\mathbf{r}_a} + (1-Q_c)u_c^2\sigma_c^T e^{i\mathbf{h}\cdot\mathbf{r}_c}}{u_a^2\sigma_a^T + u_c^2\sigma_c^T}, \quad (11.74)$$

which may be generalized for a unit cell with an arbitrary number of i atoms

$$F^h e^{2\pi i P^h} = \frac{\sum_i (1-Q_i) u_i^2 \sigma_i^T e^{i\mathbf{h}\cdot\mathbf{r}_i}}{\sum_i u_i^2 \sigma_i^T}. \tag{11.75}$$

Equation (11.75) is the XSW *structure factor for valence-electron emission.* Note that both the bond polarities and photoelectron cross sections appear in Eq. (11.75).

The main difference in the expression for the coherent fraction and coherent position in the case of the photo-excitation from the valence band comparing to the photoexcitation from the core is coming from the contribution of the *product* of the cross-sections $\sigma_{a,c}^T$ and parameters $u_{a,c}^2$ that are determined by the bond polarity value α_p (11.59). Substituting these values into expression (11.74) we have for the coherent fraction and position for an arbitrary reflection $\mathbf{h}$

$$\begin{aligned} F^h &= \sqrt{\gamma_a^2 + \gamma_c^2 + 2\gamma_a\gamma_c \cos[\mathbf{h}(\mathbf{r}_c - \mathbf{r}_a)]}, \\ \tan 2\pi\ P^h &= \frac{\gamma_a \sin(\mathbf{h}\mathbf{r}_a) + \gamma_c \sin(\mathbf{h}\mathbf{r}_c)}{\gamma_a \cos(\mathbf{h}\mathbf{r}_a) + \gamma_c \cos(\mathbf{h}\mathbf{r}_c)}, \end{aligned} \tag{11.76}$$

where parameters γ_a and γ_c are determined by

$$\begin{aligned} \gamma_a &= (1-Q_a)\frac{(1+\alpha_p)\sigma_a^T}{(1+\alpha_p)\sigma_a^T + (1-\alpha_p)\sigma_c^T}, \\ \gamma_c &= (1-Q_c)\frac{(1-\alpha_p)\sigma_c^T}{(1+\alpha_p)\sigma_a^T + (1-\alpha_p)\sigma_c^T}. \end{aligned} \tag{11.77}$$

For the case of a heteropolar bond, the anions and cations have different atomic cross-sections, and charge is transferred from the less electronegative cation to the more electronegative anion. As the positions of the anion and cation are known ($\mathbf{h}\cdot\mathbf{r}_a = -\pi/4$ and $\mathbf{h}\cdot\mathbf{r}_c = \pi/4$ for the (111) reflections), we may use the XSW structure factor of Eq. (11.74) in the dipole approximation to derive an expression for the coherent positions and fractions for the XSW valence electron yield of the zinc blende semiconductors. Due to the symmetry of the zinc blende structure, the (-1-1-1) reflections will have the same coherent fractions as the (111) reflections, but the coherent positions will be of opposite sign. For the (111) reflection the result is

$$F^{111} = \frac{\sqrt{(1+\alpha_p)^2 \left(\sigma_a^T\right)^2 + (1-\alpha_p)^2 (\sigma_c^T)^2}}{(1+\alpha_p)\sigma_a^T + (1-\alpha_p)\sigma_c^T} \tag{11.78}$$

and

$$\tan 2\pi\ P^{111} = -\frac{(1+\alpha_p)\sigma_a^T - (1-\alpha_p)\sigma_c^T}{(1+\alpha_p)\sigma_a^T + (1-\alpha_p)\sigma_c^T}. \tag{11.79}$$

This is an important result. We see, that in dipole approximation there are two independent parameters, the bond polarity coefficient α_p and the cross-section ratio σ_c^T/σ_a^T, that are contributing to the expression for the coherent fraction and coherent position. If the bond polarity value α_p is known from theory, then the cross-section ratio σ_c^T/σ_a^T can be determined from the second equation (11.79) and vice versa. The valence band of GaAs, InP and NiO crystals has been analyzed in this way and the results have been published in 2001.[42]

11.9. Summary

The matrix element for the PE is usually treated in a first-order approximation (dipole approximation). It holds astonishingly well even for hard X-rays with a wavelength much shorter than atomic dimensions as far as the magnitude of the transition matrix element is concerned. However, higher-order multipole terms introduce a deviation from the highly symmetric dipole emission profile. The forward–backward asymmetry caused already by the second-order multipole terms (dipole–quadrupole) cannot be neglected when the photoelectron is emitted by the action of an XIF, i.e., by the coherent action of two X-ray waves traveling in different directions. It has to be taken into account for the XSW analysis when analyzing differential, non-angularly integrated photoelectron signals.

To identify which atom of a crystal contributes to the density of states of a valence band, resonant photoelectron spectroscopy is traditionally used. However, the corresponding theory is not simple. Using the site-specific XSW technique is an elegant alternative and has been successfully employed several times for binary (see Chapters 12 and 26) and ternary compounds.[43]

References

1. A. Bechler and R. H. Pratt, *Phys. Rev. A* **39** (1989) 1774; **42** (1990) 6400.
2. J. W. Cooper, *Phys. Rev. A* **42** (1990) 6942; **45** (1992) 3362; **47** (1993) 1841.
3. B. Krässig, M. Jung, D. S. Gemmell, E. P. Kanter, T. LeBrun, S. H. Southworth and L. Young, *Phys. Rev. Lett.* **75** (1995) 4736; M. Jung, B. Krässig, D. S. Gemmell, E. P. Kanter, T. LeBrun, S. Southworth and L. Young, *Phys. Rev. A* **54** (1996) 2127; B. Krässig *et al. Phys. Rev. A* **67** (2003) 022707.

4. H. Sato, *et al.*, *Phys. Rev. Lett.* **93** (2004) 246404; C. Dallera, G. Panaccione, G. Paolicelli, B. Cowie, J. Zegenhagen and L. Braicovich, *Appl. Phys. Lett.* **85** (2004) 4532; K. Kobayashi *et al. Appl. Phys. Lett.* **83** (2003) 1005; P. Torelli *et al.*, *Rev. Sci. Instrum.* **76** (2005) 023909; for a review see J. Zegenhagen and C. Kunz (eds.), in *Proc. Workshop on Hard X-Ray Photoelectron Spectroscopy*, Grenoble, 2003, *Nucl. Instrum. Meth. Phys. Res. A* **547** (2005).
5. B. W. Batterman, *Phys. Rev. Lett.* **22** (1969) 703.
6. J. Zegenhagen, *Surf. Sci. Rep.* **18** (1993) 199.
7. I. A. Vartaniants and M. V. Kovalchuk, *Rep. Prog. Phys.* **64** (2001) 1009.
8. L. E. Berman and M. J. Bedzyk, *Phys. Rev. Lett.* **63** (1989) 1172.
9. I. A. Vartanyants and J. Zegenhagen, *Solid State Commun.* **113** (2000) 299; (Erratum) **115** (2000) 161.
10. I. A. Vartanyants and J. Zegenhagen, *Nuovo Cimento* **19D** (1997) 617.
11. I. A. Vartanyants and J. Zegenhagen, *Phys. Status Solidi B* **215** (1999) 819.
12. I. A. Vartanyants, T.-L. Lee, S. Thiess and J. Zegenhagen, *Nucl. Instrum. Meth. Phys. Res. A* **547** (2005) 196.
13. C. J. Fisher, R. Ithin, R. G. Jones, G. J. Jackson, D. P. Woodruff and B. C. C. Cowie, *J. Phys. Condens. Matter* **10** (1998) L623.
14. G. J. Jackson, B. C. C. Cowie, D. P. Woodruff, R. G. Jones, M. S. Kariapper, C. Fisher, A. S. Y. Chan and M. Butterfield, *Phys. Rev. Lett.* **84** (2000) 2346.
15. F. Schreiber, K. A. Ritley, I. A. Vartanyants, H. Dosch, J. Zegenhagen and B. C. C. Cowie, *Surf. Sci. Lett.* **486** (2001) L519.
16. J. J. Lee, C. J. Fisher, D. P. Woodruff, M. G. Roper, R. G. Jones and B. C. C. Cowie, *Surf. Sci.* **494** (2001) 166.
17. E. J. Nelson, J. C. Woicik, P. Pianetta, I. A. Vartanyants and J. W. Cooper, *Phys. Rev. B* **65** (2002) 165219.
18. N. Hertel, G. Materlik and J. Zegenhagen, *Z. Phys. B Condens. Matter* **58** (1985) 199.
19. J. Cooper and R. N. Zare, in *Lectures in Theoretical Physics*, Vol. XI-C, eds. S. Geltman, K. T. Mahanthappa and W. E. Brittin (Gordon and Beach, Science Publishers, New York–London–Paris, 1968).
20. See for e.g., reviews of theoretical and experimental studies of the atomic photoionization: A. F. Starace, in *Handbuch der Physik*, Vol. XXXI, ed. W. Mehlhorn (Springer-Verlag, Berlin, 1982), pp. 1–121; J. A. R. Samson, pp. 123–213; V. Schmidt, *Rep. Prog. Phys.* **55** (1992) 1483.
21. H. A. Bethe and R. W. Jackiw, *Intermediate Quantum Mechanics*, 3rd edn. (Benjamin Cummings, Reading, New York, 1986), Chap. 12.
22. M. B. Trzhaskovskaya, V. I. Nefedov and V. G. Yarzhemsky, *Atom. Data Nucl. Data Tables* **77** (2001) 97; **82** (2002) 257; M. B. Trzhaskovskaya, V. K. Nikulin, V. I. Nefedov and V. G. Yarzhemsky, *Atom. Data Nuclear Data Tables* **92** (2006) 245.
23. S. Thiess, C. Kunz, B. C. C. Cowie, T.-L. Lee, M. Renier and J. Zegenhagen, *Solid State Commun.* **132** (2004) 589.
24. A. Derevianko, W. R. Johnson and K. T. Cheng, *Atom. Data Nucl. Data Tables* **73** (1999) 153.

25. A. Derevianko *et al.*, *Phys. Rev. Lett.* **84** (2000) 2116.
26. A. A. Akhiezer and V. B. Berestetskii, *Quantum Electrodynamics* (Interscience, New York, 1965); V. B. Berestetskii, E. M. Lifshitz and L. P. Pitaevskii, *Relativistic Quantum Theory* (Pergamon, New York, 1971).
27. L. D. Landau and E. M. Lifshitz, *Quantum Mechanichs — Nonrelativistic Theory*, 2nd edn. (Pergamon Press, Oxford, 1965).
28. A. Jablonski, F. Salvat and C. J. Powell, *NIST Electron Elastic Scattering Cross-Section Database*-Version 3.0 (National, Institute of Standarts and Technology, Gaithersburg, MD 2002); Available at http://www.nist.gov/srd/nist64.cfm.
29. A. R. Edmonds, *Angular Momentum in Quantum Mechanics* (Princeton University Press, Princeton, N.J., USA 1957).
30. I. I. Sobel'man, *An Introduction to the Theory of Atomic Spectra* (Pergamon Press, Oxford, 1972).
31. H. Wagenfeld, *Phys. Rev.* **144** (1966) 216.
32. G. Hildebrandt, J. D. Stephenson and H. Wagenfeld, *Naturforsch A* **30** (1975) 697 ; J. D. Stephenson, *Naturforsch A* **30** (1975) 1133.
33. S. T. Manson, *J. Electron Spectrosc.* **1** (1972/1973) 413; **2** (1973) 206; **2** (1973) 482.
34. One of the widely used code for EXAFS analysis FEFF is one of the possible sources for calculation of the phase shifts, see, for e.g., http://leonardo.phys.washington.edu/feff/. Accessed Sept. 13, 2012.
35. A. Gerlach, F. Schreiber, S. Sellner, H. Dosch, I. A. Vartanyants, B. C. C. Cowie, T.-L. Lee and J. Zegenhagen, *Phys. Rev. B* **71** (2005) 205425.
36. W. A. Harrison, *Electronic Structure and the Properties of Solids* (Freeman, San-Francisco, 1980), Chaps. 3 and 7.
37. N. W. Ashcroff and N. D. Mermin, *Solid State Physics* (Holt, Rinehart and Winston, New York, 1976), Chap. 10, Appendix F.
38. H. A. Bethe and E. E. Salpeter, *Quantum Mechanichs of One- and Two-Electron Atoms* (Plenum, New York, 1977), Chap. 4.
39. W. Braun, A. Goldmann and M. Cardona, *Phys. Rev. B* **10** (1974) 5069.
40. V. G. Aleshin and Yu. N. Kucherenko, *J. Electron Spectrosc.* **8** (1976) 411.
41. A. L. Fetter and J. D. Walecka, *Theoretical Mechanics of Particles and Continua* (McGraw-Hill, New York, 1980), Chap. 10.
42. J. C. Woicik, E. J. Nelson, D. Heskett, J. Warner, L. E. Berman, B. A. Karlin, I. A. Vartanyants, M. Z. Hasan, T. Kendelewicz, Z. X. Shen and P. Pianetta, *Phys. Rev. B* **64** (2001) 125115.
43. S. Thiess, T. L. Lee, F. Bottin and J. Zegenhagen, *Solid State Commun.* **150** (2010) 553.